

Silver Anniversary Paper, Division 4

Porosity in Castings

R. Monroe

Steel Founders' Society of America, Crystal Lake, Illinois

Copyright 2005 American Foundry Society

ABSTRACT

Porosity may be the most persistent and common complaint of casting users. Forgings, machined parts and fabrications are able to avoid porosity with ingot cast feedstock, mechanical processing and automated inspection of simple shapes. Porosity in castings contributes directly to customer concerns about reliability and quality. Controlling porosity depends on understanding its sources and causes. Significant improvements in product quality, component performance, and design reliability can be achieved if porosity in castings can be controlled or eliminated.

Porosity in castings is due to bubbles being trapped during solidification. Porosity sources include entrapped air during filling, centerline shrinkage that occurs during the final solidification, blowholes from unvented cores, reactions at the mold wall, dissolved gases from melting and dross or slag containing gas porosity.

This paper is an update to a presentation to the 1980 AFS Casting Congress concerning gas holes in castings.⁽¹⁾ This update will seek to review that work and try to articulate a framework for understanding and controlling porosity in castings. A paper from the 1980 AFS presentation was published in 1981.⁽²⁾

POROSITY SOURCES

AIR ENTRAINMENT

Filling of the mold cavity with molten metal is basic to casting production. One source of porosity in castings is a failure to eliminate all the air in the mold cavity. Most often this porosity appears to be a misrun or incomplete casting. In skin forming alloys when the filling event is chaotic, air bubbles can be entrapped in the casting. Sometimes the air bubbles deflate, leaving the oxidized skin. As a simple example illustrating the basic relationships of size, pressure and temperature, entrapped air bubbles are a good starting place.

Suppose an air bubble is trapped in a casting during pouring and is unable to escape before solidification. How big would it be? If the air bubble is originally 10 mm in diameter (a little larger than 3/8 in. and a volume of about 0.5 ml), the higher temperature of the molten metal will cause the air bubble to expand initially and then contract until the metal freezes. The size change due to temperature at solidification can be calculated using Charles' Law by multiplying the original volume of the bubble by the ratio of the final temperature divided by the initial temperature.

$$\text{Final volume} = \text{initial volume} * (\text{final temperature} / \text{initial temperature})$$

(A) Charles' Law^(3, p. 282)

Temperature must be in absolute terms. For example, room temperature is usually given as 298°K (25°C or 77°F). For steel, the final temperature of 1773°K (1500°C or 2732°F) gives a volume of 3 ml (18 mm in diameter or almost 3/4 in.). Other metals are shown in Table 1.

The size of the final bubble must not only be adjusted for temperature change but also for pressure. Just like the pressure increases as you go deeper in water, the liquid metal pressure (metallostatic head) increases as you go lower in the casting.

Table 1. Bubble Size of Entrained Air Adjusted for Temperature⁽⁴⁾

Bubble	Temp. (C°)	Temp. (F°)	Volume (ml)	Dia. (mm)	Dia. (in.)
Original	25	80	0.52	10.0	0.393
Steel	1500	2730	3.11	18.1	0.713
Cast Iron	1150	2100	2.50	16.8	0.663
Aluminum	600	1100	1.53	14.3	0.56
Brass or Bronze	1050	1900	2.36	16.5	0.651

The pressure can be calculated from the density of the metal and the depth from the top of the sprue. For example, at 200 mm down in the casting (about 8 in.) the pressure in steel is the density (7850 kg/m³) times the depth (0.2 m) or 1570 kg/m² (0.15 atm gage or 1.15 atm absolute). Using Boyle's Law, the size change due to pressure can be calculated by multiplying the initial volume of the bubble by the ratio of the initial pressure divided by the final pressure.

$$\text{Final volume} = \text{initial volume} * (\text{initial pressure} / \text{final pressure})$$

(B) Boyle's Law^(3 p. 282)

Normal atmospheric pressure is one atmosphere. For steel, this pressure due to the metalstatic head reduces the larger volume of 3 ml due to temperature to 2.7 ml (17 mm in diameter or about 5/8 in). Other metals are shown in Table 2.

Table 2. Bubble Size of Entrained Air adjusted for Depth of 200 mm^(4, p. 462)

Original	Density (kg/m ³)	Pressure (atm)	Volume (ml)	Diameter (mm)	Diameter (in.)
Steel	7800	1.15	2.70	17.3	0.68
Cast Iron	7200	1.14	2.19	16.1	0.63
Aluminum	2800	1.05	1.46	14.1	0.55
Brass or Bronze	8800	1.17	2.02	15.7	0.62

Because the entrapped air will react with the molten metal, the pore size will actually become smaller as the oxygen in the air forms oxides with the molten metal. In steel and aluminum, all the oxygen would be consumed and the hole would shrink in volume about 20%. This would lead to a final volume of 2.1 ml in steel and 1.2 ml in aluminum. In iron, the oxygen might either form an oxide or carbon monoxide. If the oxygen formed carbon monoxide, the size of the pore would not change.

The comparatively low pressures and high temperatures of metal casting operations make most gas porosity calculations relatively accurate using the Ideal Gas Law.

$$\text{Pressure} * \text{Volume} = \text{Moles} * \text{Gas Constant} * \text{Temperature} (PV = nRT)$$

(C) Ideal Gas Law^(3, p. 283)

The Ideal Gas Law combines the effects of Charles' and Boyle's Laws with volumes increasing at higher temperatures and decreasing at higher pressures. The number of molecules of gas is stated as moles, the mass of gas divided by the molecular weight gives the number of moles. For example, nitrogen is a diatomic gas, N₂, and has an atomic weight of 14 or molecular weight of 28. For nitrogen gas, one mole would be 28 grams and contain Avagadro's number of molecules, 6.023 * 10²³. Air is made of approximately 80% nitrogen and 20 % oxygen for an average molecular weight of 28.8.

The gas constant, R, makes all the units work out and is 0.082 (atm*I)/(mole*°K). The air bubble of the original example, 10mm in diameter, has a volume of 0.5 ml, and contains 0.00002 moles or 0.0006 grams of air (0.0000014 lbs).

BLOW HOLES

Closely related to air bubbles trapped during filling are gas bubbles that are blown into the liquid from a core or mold much like a kid blowing bubbles using a straw. All porosity is the result of bubble formation and all bubbles follow a basic relationship.

$$\text{Pressure of gas-forming bubble} > \text{Pressure inside the liquid} + 2 * \text{surface tension} / \text{radius of bubble}$$

(P_b > P_{Hd} + 2σ / r)...(D)^(2, p. 676)

If the local gas pressure in a mold or core exceeds the local metallostatic head of the liquid, a bubble will be blown into the liquid metal. An example of this can be seen in a series of trials where a glass funnel filled with bonded sand with an attached copper tube and pressure sensor was molded in the drag of a plate mold shown in Figure 1.^(2, p. 678) Since the gas could not escape, pressure in the funnel increased as measured by the sensor until the pressure exceeded the metallostatic head and blow holes were formed. A typical pressure and temperature profile of these trials is shown in Figure 2.^(2, p. 680)

The pressure increased to slightly above the metallostatic head until a bubble began to form and then the pressure would fall as gas entered the bubble and the radius of the bubble increased. Finally, the bubble would break away and float up through the riser and could be seen emerging from the riser. The pressure would then begin to rise again until the next bubble would form. The solidifying metal would form a bubble starting point and this would reduce the pressure variation until solidification began and the pressure required forming and releasing a bubble increased. Finally the solidifying metal would stop bubble formation and the pressure would rise until the system leaked.

The average pressure during bubbling in iron casting trials is shown in Figure 3.^(2, p. 685) The pressure line shown in Figure 3 is calculated from the metallostatic head pressure of cast iron. Low head pressure occurred during mold failures while low pressures occurred because of leaks in the system. These conditions show clearly that equation D describes the pressures required, even the slight excess pressure to begin a bubble. Leaks in the pressure measurement system were like vents, preventing blowholes or bubbling by allowing the gas to escape at lower pressures.

The pressure measured to form a blowhole can be compared to the metallostatic pressure based on the sprue height for the casting reported in the literature. These pressures are given in Table 3.^(2, p. 681-682) The radiographic determination of porosity showed large blowholes in all bubbling plates in aluminum and iron casting. In steel castings, bubbling plates had more dispersed general porosity and not a single large trapped bubble. The pressure required to form a blowhole must exceed the metallostatic head exerted by the sprue.

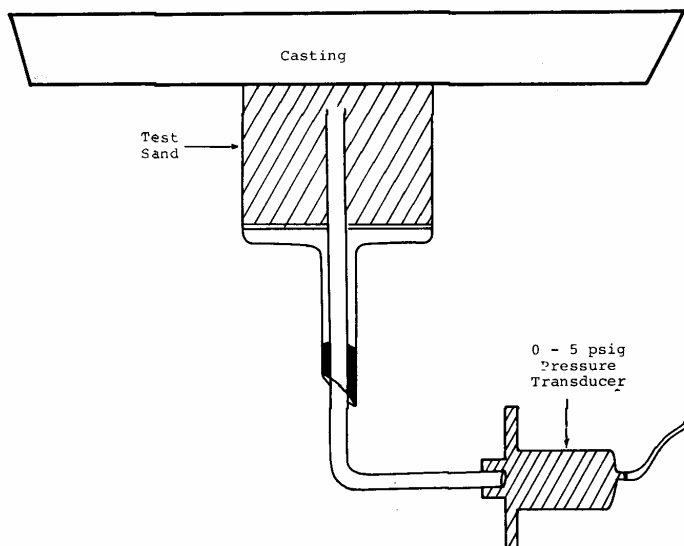


Figure 1. Pressure measurement in test castings.

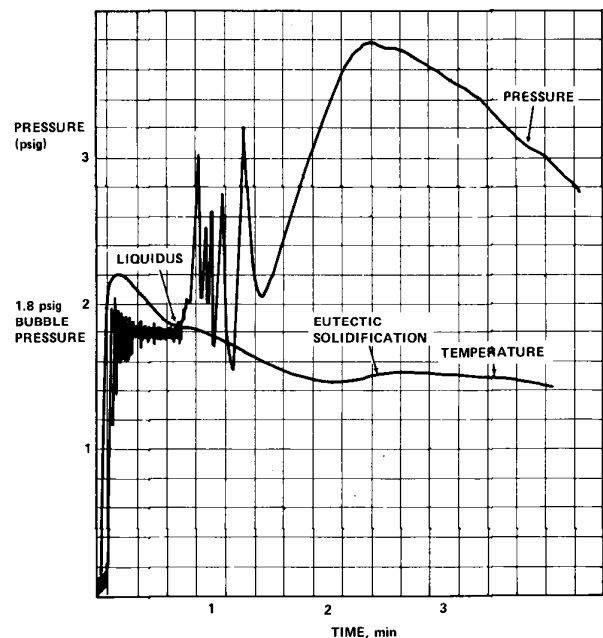


Figure 2. Temperature and pressure profile from furan mold and core in cast iron.

Table 3. Pressure of Bubble Formation in Plate Castings

Pressure Atm	Steel	Cast Iron	Aluminum
Sprue pressure calculated	0.082–0.115	0.089–0.100	0.035–0.040
Bubble pressure measured	0.075–0.085	0.085–0.128	0.038–0.042

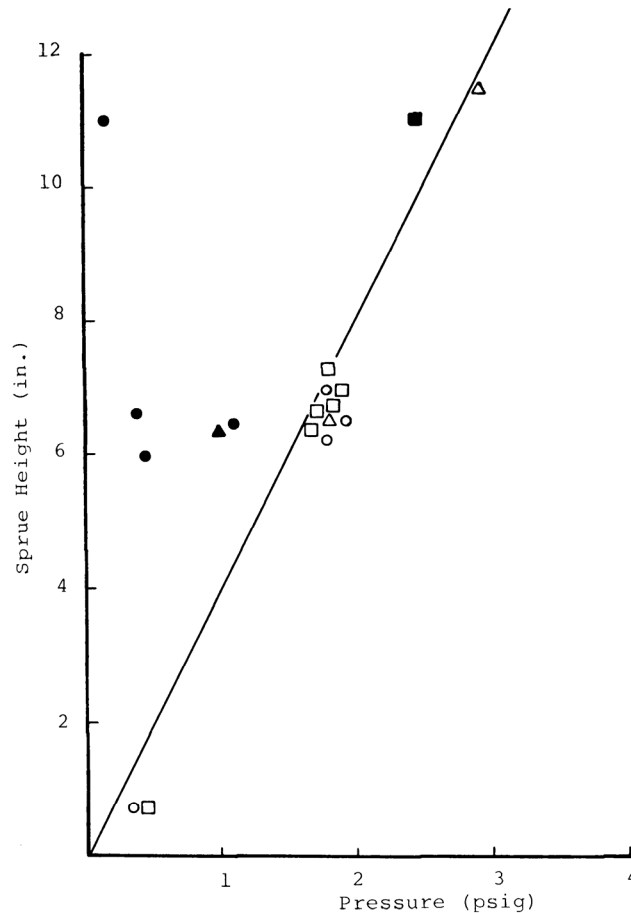


Figure 3. Effect of sprue height on pressure required to form a bubble in cast iron. (Open symbols were castings with blowholes; closed symbols were castings without blowholes.)

To calculate the pressure of gas in a mold or core it is necessary to know how much gas is created at the mold metal interface. The binder and other additives vaporize while the air in the void space expands and the air in the cavity must escape through the voids. If we assume that the air in the cavity escapes through the vents and out of the risers or gating flow offs, then the expansion of air, decomposition and vaporization of the binder are the source of gas at the interface. Since the mold or core typically contains 50% by volume porosity, as calculated above each volume (ml or cm³), contains only half a volume (0.5ml) of air (0.00002 moles). The amount of gas generated from binder can be estimated from the loss on ignition (LOI %) as a function of temperature from Figure 4.^(2, p. 686) At 500°C three quarters of the volatiles in the sand mixture are removed. At a typical mold or core density of 1.5 g/ml and a 1% binder level, there is 0.015g of binder/ ml of mold or core. Using the molecular weight of methane (CH₄, molecular weight 16) then the gas generated at 500°C would be 0.0007 moles for a total gas amount of 0.00072 moles or using equation C, 18 ml of gas at STP or 45 ml at 500°C generated for each ml of mold above 500 °C.

Approximating the temperature profile in the sand by holding the mold metal interface at the characteristic temperature of each metal from Table 1, using a typical thermal diffusivity for the mold of 0.004 cm²/sec, and considering the mold as an infinite solid, it is possible to calculate the temperature rise in the sand. Since the measurement allows the gas to cool substantially, the volume of gas is calculated using standard conditions. Using the LOI information in Figure 4, the

composition of gas reported for the molecular weight and the calculated temperature in the mold, the gas generated can be calculated as given in Table 4a for phenolic urethane no bake, PUNB and Table 4b for furan no bake, FNB.

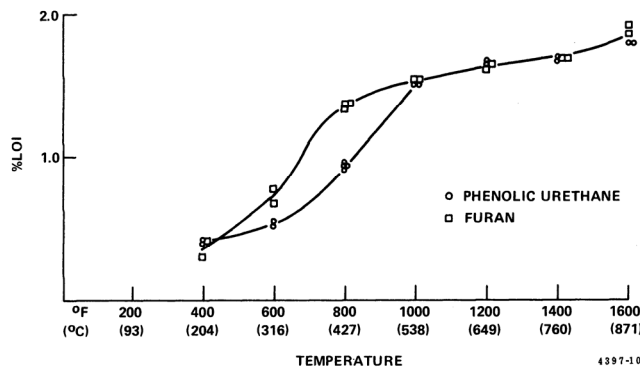


Figure 4. Loss of ignition of mold and core sand at various temperatures.

Table 4a. Total Gas Evolved and Rate of Gas Evolution Calculated With PUNB 2.0% LOI

Time (s)	Steel Total gas (ml/cm ²)	Steel Rate of gas (ml/cm ² /s)	Cast Iron Total gas (ml/cm ²)	Cast Iron Rate of gas (ml/cm ² /s)	Brass Total gas (ml/cm ²)	Brass Rate of gas (ml/cm ² /s)	Aluminum Total gas (ml/cm ²)	Aluminum Rate of gas (ml/cm ² /s)
15	6.68	0.45	4.83	0.32	4.47	0.30	1.44	0.10
30	9.45	0.18	6.84	0.13	6.32	0.12	2.04	0.04
60	13.36	0.13	9.67	0.09	8.93	0.09	2.88	0.03
90	16.36	0.10	11.84	0.07	10.94	0.07	3.53	0.02
120	18.90	0.08	13.68	0.06	12.65	0.06	4.09	0.02

Table 4b. Total Gas Evolved and Rate of Gas Evolution Calculated With FNB 2.0% LOI

Time (s)	Steel Total gas (ml/cm ²)	Steel Rate of gas (ml/cm ² /s)	Cast Iron Total gas (ml/cm ²)	Cast Iron Rate of gas (ml/cm ² /s)	Brass Total gas (ml/cm ²)	Brass Rate of gas (ml/cm ² /s)	Aluminum Total gas (ml/cm ²)	Aluminum Rate of gas (ml/cm ² /s)
15	7.59	0.51	5.72	0.38	5.33	0.36	1.86	0.12
30	10.74	0.21	8.09	0.16	7.54	0.15	2.62	0.05
60	15.18	0.15	11.44	0.11	10.66	0.10	3.71	0.04
90	18.59	0.11	14.01	0.09	13.06	0.08	4.55	0.03
120	21.47	0.10	16.19	0.07	15.09	0.07	5.25	0.02

This calculated gas evolution can be compared with the measured rates from the literature.^(2, p. 681) The binder levels and residual in the reclaimed sands used in the earlier trials is higher than current levels. Table 5 compares the calculated values of Table 4 with the measured values from prior work.^(2, p. 681)

Table 5. Total Gas Evolved in One Minute (ml/cm²)

Binder/LOI %	Steel	Cast Iron	Aluminum
PUNB Calculated 2.00	13.36	9.67	2.88
PUNB 1.78	9.0	--	1.0
PUNB 3.07	15.6	12.4	1.2
FNB Calculated 2.00	15.18	11.44	3.71
FNB 1.89	15.7	9.5	1.1
FNB 2.57	21.2	13.9	1.3

The peak gas evolution rate will depend not only on the metal cast, its pouring temperature, the type of mold and binder, but also on the amount of binder. Higher binder levels will increase peak evolution rates. The values for total gas evolved for 15 seconds from Table 4 were used to calculate the peak rate and the results are shown versus experimental measures in Table 6. The simple engineering calculation will give an unrealistic high peak rate at small times since it assumes an instantaneous fill with immediate gas evolution. The measured values are also limited in accuracy since the volume of the sampling system and the distance from the mold to the measurement provides some dampening. In any case the agreement of calculated and observed rates was good for an engineering calculation and suggests that numerical modeling should be possible. A numerical model could provide a more accurate temperature distribution, gas evolution rate, and pressure distribution.

Table 6. Peak Gas Evolution Rate (ml/s/cm²)

Binder/LOI %	Steel	Cast Iron	Aluminum
PUNB Calculated 2.00	0.44	0.32	0.10
PUNB 1.78	0.22	--	0.03
PUNB 3.07	0.52	0.37	0.06
FNB Calculated 2.00	0.50	0.38	0.12
FNB 1.89	-	0.34	0.06
FNB 2.57	-	0.65	0.04

Earlier work on surface quality also measured gas evolution rates using a variety of chemically bonded systems. The total gas evolution rate and total gas evolved was determined using a glass funnel capture system and an irregular gear poured in gray iron. The gas evolution rates can be used to calculate the gas evolution from the sand mixtures similar to the procedure of Tables 5 and 6. These are given in Table 7.^(5, p. 610)

Table 7. Total Gas Evolved and Rate of Gas Evolution for Cast Iron

Binder	LOI %	Peak gas evolution rate ml/cm ² /s	Total gas evolved in one minute ml/cm ²
Alkyd Urethane new	1.3	0.73	26
PUNB new	1.5	0.24	10
PUNB reclaim mold	3.3	0.73	30
PUNB reclaim core	2.4	0.48	22
Phenolic shell	3.4	0.73	20
Phenol Formaldehyde	1.5	0.48	18
Furan new	1.5	0.39	15
Furan reclaim	2.7	0.70	25
Sodium Silicate ester	1.0	0.21	9
Calculated PUNB	2.0	0.32	10
Calculated FNB	2.0	0.38	11

Several tests were developed to measure the gas evolved from different sand mixtures by heating a small sample to relatively high temperatures.^(6, p. 11-10) The rate of gas evolution based on the weight of the sample was thought to be indicative of the gas evolved during casting. Unfortunately, no consistent results useful for sand quality control or engineering came from these standard tests. In fact, the standard tests sometimes gave results that were not consistent with casting trials. The disparity between the gas evolution rate procedure using a small sample and a test temperature of 1010°C (1850°F) and the gas evolution measured in the molds led to subsequent work to resolve the differences.

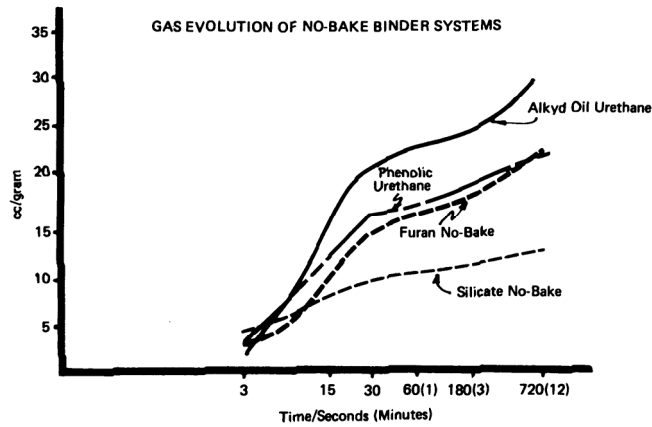


Figure 5. Gas evolution test of no-bake binder systems at 1010°C (1850°F).

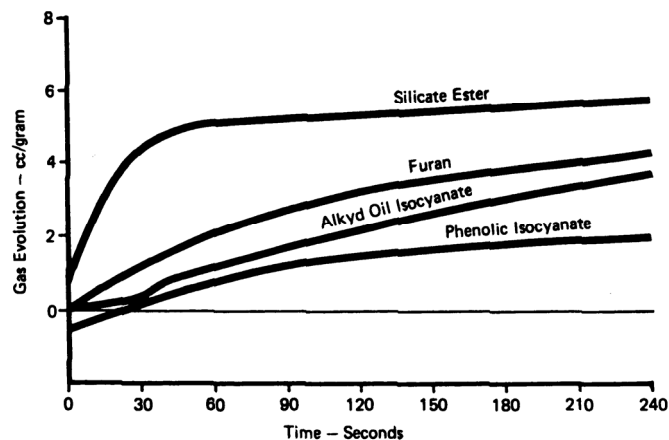


Figure 6. Modified gas evolution test of no-bake binder systems at 370°C (700°F).

For example, several sand binder formulations were tested using the common procedures and the results are given in Figure 5.^(7, p. 370) This shows phenolic urethane with a slightly higher gas evolution than furan though the mold trials reported in Table 6 and 7 show lower rates and totals for phenolic urethane. The LOI results suggest that at lower temperatures, the results will be different, with the greatest difference at about 370°C (700°F) as seen in Figure 4. A modified procedure was developed using a larger sand sample, a lower temperature, 370°C (700°F), a shorter test, and a procedure to capture moisture gave results more representative of the mold-measured results. The results of this modified test are consistent with casting trials and are shown in Figure 6.^(7, p. 371)

The pressure at the mold-metal or core metal interface rises because the air being replaced in the mold must be evacuated and removed, the air in the mold or core heats up, and the binder or other mold materials boil, decompose and heat up. The mold or core materials prevent the immediate release of the gas pressure. The resistance of the mold or core depends on the distance to the vent or free surface, the smallest cross section and lowest permeability. Pressure at the mold metal interface can be calculated from the volume of gas that must be removed from the interface and the resistance of the mold to gas flows. The resistance to gas flow through sand molds and cores is measured as permeability.

$$\text{Permeability} = (\text{volume of gas} \times \text{thickness of sand}) / (\text{gas pressure} \times \text{area} \times \text{time}) \dots \dots \dots (E)^{(6, p. 6-4)}$$

On a flat mold surface the calculation would be straightforward by solving for gas pressure. The expression for permeability given can be rearranged to calculate pressure.

$$\text{Gas Pressure} = (\text{gas evolution rate} \times \text{thickness of mold}) / \text{permeability} \dots (F)^{(8, p. 6)}$$

If the peak gas evolution rate is 0.5 ml/s/cm² and the permeability is 50, then the calculated maximum gas pressure for a mold 200 mm thick on a flat mold surface is 0.012 atm or 0.17 psig. Since the gas at the interface is hot, it may be more appropriate to use a gas evolution volume at 500°C with a rate of 1.5 ml/s/cm². For the conditions given, the pressure would increase to 0.035 atm or 0.51 psig. The metal head pressure for steel at 200 mm was calculated to be 0.15 atm, not enough to suppress bubble formation at the mold metal interface at the peak rate. Doubling the permeability would halve the peak pressure.

The most significant factor is the distance to atmosphere, the distance from the mold-metal interface to the mold surface or vent. If the mold drag is sitting on sand the distance from the center of the mold-metal interface to a surface of the mold could be considerable. If instead of 200 mm (about 4 in.) the distance were 400 mm, the pressure would be twice or 0.07 atm or 1.0 psig. The reported relationship between gas pressure and permeability are shown in Figure 7.^(2, p. 674) Agreement is good considering the differences in sand mixture formulations. The leaking system in Figure 3 also shows a minimum pressure of about 0.3 psig consistent with these calculations.

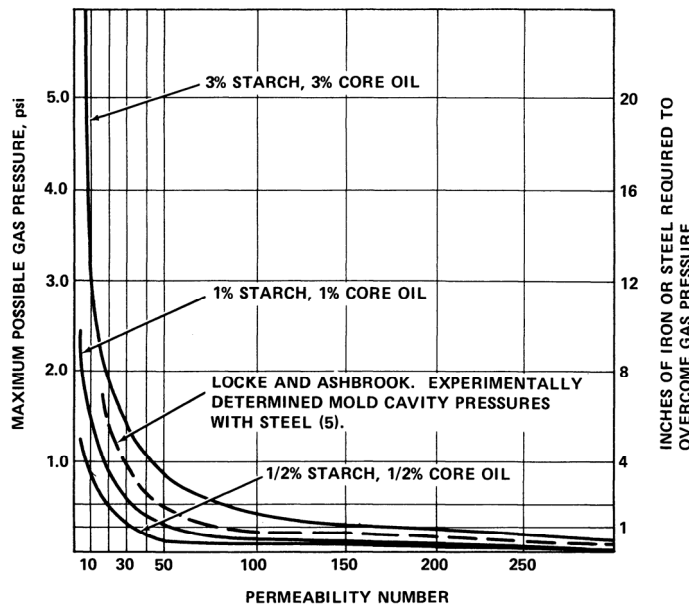


Figure 7. Permeability and gas pressure on flat sand/metal interface in iron or steel.

The pressure will change dramatically if incomplete mixing or other operational conditions results in areas with significantly higher LOIs. This effect is made worse if the permeability of the mold is degraded locally. The failure to control the fines in the sand system with their higher LOI can clearly cause gas holes.

Another possible problem is the unvented drag. Molds are often placed on sand or other impermeable bedding prior to pouring the mold. As shown above, the distance to vent or mold wall is significant in calculating the peak pressures. Gas evolved in the drag in the center of the casting is like gas evolved in a core with a lot of surface area exposed to the metal. In either case, the gas may not be able to escape and instead form a bubble site. This active site once initiated may continue to bubble until the casting solidifies resulting in gas porosity. This is one explanation of why higher pouring temperatures may sometimes eliminate porosity. By delaying final solidification, the peak gas evolution rate is over before solidification starts. Bubbling from cores or the drag has been clearly demonstrated in castings.^(9, p. 22) Drag porosity must form during solidification of the casting surface since prior to that it would float away and after that it would be unable to form.

Additional tests pouring a horizontal plate and monitoring fill show the entrapment of air and the development of bubbles from the mold or coating. Excess coating made the filling less rapid and chaotic but allowed more trapped gas porosity. Bubbles of trapped gas occur in filling in less than 2 seconds, while blowholes from the mold formed in 16 to 18 seconds after filling.^(10, p. 6)

Similar to the problem of the unvented drag is the situation with a core. In a core, the gas evolved on the core surface must be removed through the core print. This changes the equation (F) for pressure.

$$\text{Gas Pressure} = (\text{gas evolution rate} * \text{surface area of core-metal interface} * \text{distance to vent}) / (\text{permeability} * \text{core print area}) \text{ (G)}^{(8, p. 6)}$$

For a 25mm x 25mm square bar core extending 25mm into the cavity and vented 25mm from the print, we can recalculate a peak pressure of 0.022 atm or 0.32 psig. If the core is extended to 125 mm into the cavity, the peak pressure calculates as 0.091 atm or 1.34 psig. If the vent is 125mm from the print then the pressures are increased by a factor of five, or in the last case, 0.46 atm (6.7 psig). These calculations can be compared to the graphs in Figure 8^(2, p. 675) showing good agreement. A large core with limited core print area is always prone to blowholes.^(11, p. 201)

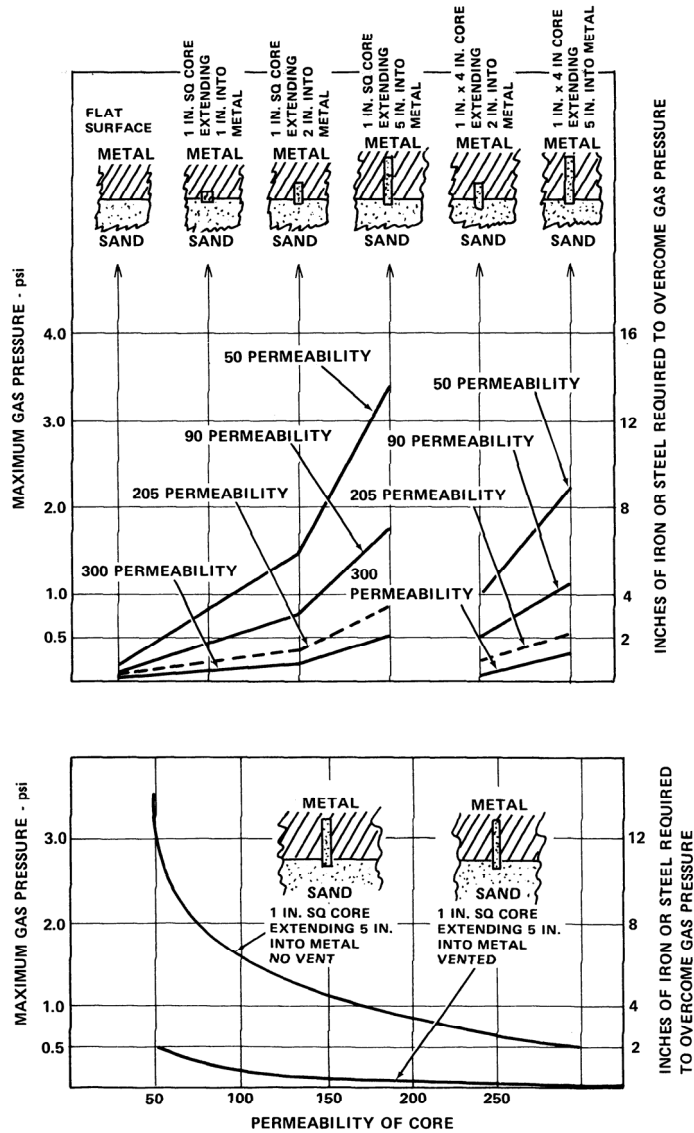


Figure 8. Permeability and gas pressure in various core configurations in iron or steel.

An example of using this approach can be shown with a test casting designed to study blowholes. A core, 30.5 cm long (12 in.) and 5.1 cm diameter (2 in.) was cast in a cylinder, 33 cm long (13 in.) and 7.6 cm (3 in.) diameter, with core prints at each end. Permeability was varied from 50 to 120, head height was raised from the standard 11.4 cm (4.5 in.) to 34.3 cm (13.5 in.), binders were 1% of various types, and core prints were enlarged from 1.9 cm (0.75 in.) to 2.54 cm (1.0 in.), 3.2 cm (1.25 in.) and 1.9 cm (0.75 in.) drilled. The casting was poured in grey iron at 1482°C (2700°F). If 5 ml/cm² of gas evolved in one minute (Table 5 for binder at 1%), then the peak pressure by Equation G for a permeability of 50, core print of 1.9 cm (0.75 in.) would be 0.136 atm. The head height at 11.5 cm (4.5 in.) would give a head pressure of 0.08 atm, not enough to prevent a blowhole and the test castings had blowholes. If a higher permeability of 120 is used the calculated core pressure decreases to 0.06 atm and should not form a blowhole. The test castings under these conditions were free of blowholes. The results of the test castings are given in Table 8 along with calculated values for pressure.^(7, pp. 372-374) The core print enlargement was calculated by adding the resistance in the core to the core print (15.2 cm (6 in.) at a permeability of 50) to the core print core (0.13 cm (0.05 in.) at a permeability of 20). The bottom row shows the results of drilling a vent through to core print and illustrates nicely the powerful effect of venting.

Table 8. Calculated Core Gas Pressures and Experimental Blowhole Results

Permeability	Core print (cm ²)	Head Height (cm)	Core pressure (atm)	Head pressure (atm)	Blowholes
50	5.7	115	0.14	0.08	Severe
120	5.7	115	0.06	0.08	Sound
50	5.7	191	0.14	0.13	Slight
50	5.7	267	0.14	0.19	Trace
50	5.7	343	0.14	0.23	Sound
50+20	5.7	115	0.15	0.08	Severe
50+20	10.1	115	0.09	0.08	Slight
50+20	15.8	115	0.05	0.08	Sound
Vented	40.5	115	0.02	0.08	Sound

In the prior calculations, it was assumed that the vent was able to operate at atmospheric pressure. It is worthwhile to consider the capacity of the vent. The maximum pressure drop along the vent is the metal head pressure; at 200mm the pressure is 0.15 atm. For the gas calculation at 500°C (932°F), the gas density from the ideal gas law is 0.00031 g/ml. For a vent with a 3mm (1/8 in) diameter and 200mm (8 in) long using the method presented in engineering handbooks, the vent would have a capacity of over 1700ml/s.^(12, p. 4-66)

If the vents are near surface and the peak gas evolution rate is 0.5 ml/s/cm², each vent could handle the peak evolution from 3400 cm² or a circle 65 cm (26 in) in diameter. This shows that venting cores at the core print is critical in avoiding gas holes in castings. The key is not the capacity of the vent but its location close to the higher gas pressure areas of the mold or at the core print. It is the resistance, mold or core permeability, to get to the vent that leads to higher pressures.

Gas tracks on the surface of castings are paths of the gas escaping the mold metal interface to the nearest vent, such as a riser. This occurs most often on the cope surface. Gas unable to get to a vent in the drag may form through wall porosity close to the edge.

OXIDES

Much of the porosity in castings is not the result of excess gas pressure forming blowholes or gas solubility forming pinholes but is the result of oxides. In fact, most of the surface or subsurface porosity is likely due to oxide formation. In steel castings, many of the reoxidation inclusions include associated porosity. Frequently when the inclusion material is removed by blasting, the associated porosity remains. Drossy, gassy areas in steel castings are often mislabeled porosity by customers.

Reoxidation in steel affects every factor required to form a bubble. The inclusion material floats higher in the casting reducing the pressure to be overcome. The less stable oxides, such as iron or manganese oxide, are reduced by carbon, forming carbon monoxide, a source of gas for bubble formation. Higher levels of oxygen locally reduce the surface tension that must be overcome to form a bubble. The reduction of surface tension due to increases in oxygen is shown in Figure 9.^(3, p. 356) Finally, oxide inclusions provide the needed nucleation sites for porosity formation.

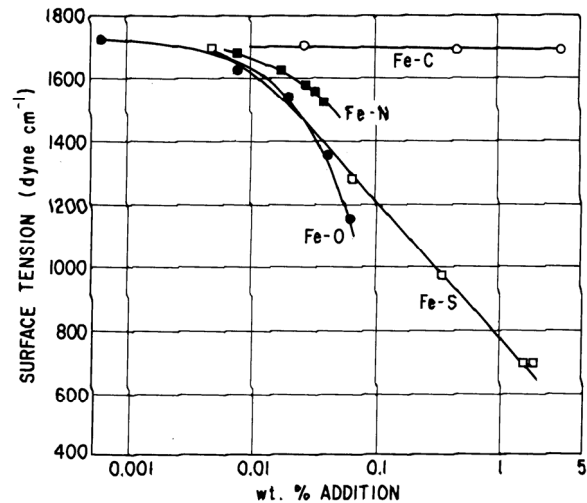


Figure 9. Effect of carbon, nitrogen, sulfur and oxygen on the surface tension of iron.

Dross or glassy oxides occur in all cast metals operations. The entrapment of this glassy material or its formation during casting often results in porosity. Control of this porosity is a matter of controlling the formation and entrapment of oxides in casting. Cast iron has sufficient carbon content so that carbon monoxide forms in preference to other oxides at the molten metal surface at normal tapping and pouring temperatures. Because of this, good casting operations are able to clean the surface of the iron prior to pouring. In steel, a continuously forming slag prevents a clean surface. Large porosity in iron castings is often labeled a slag blowhole, with some oxide or dross attached to a large porosity cavity. Fluid slag entrapment or reoxidation have been identified as sources.^(13, p. 164)

Additional work shows that pinhole formation associated with slag or dross is due to the reaction of iron oxide and carbon to form carbon monoxide. Aluminum tends to suppress the formation of iron oxide and pinhole formation. High levels of magnesium and low pouring temperatures increase dross formation and pinhole frequency. Reoxidation slag is the fundamental cause of pinholes in iron castings. If controlled pouring subsurface from slag can be achieved, pinholes are avoided.^(16, p. 75)

Dross also forms as the iron cools below 1350°C and silicon oxide replaces carbon monoxide as the preferred oxide to form. This reoxidation dross formation is a major cause of porosity in iron castings. Like steel operations, eliminating reaction with air or other oxygen sources during pouring is critical to avoiding these problems.

In aluminum operations, an oxide film forms immediately. When late inoculants are added or good practices are neglected, dross from melting or treating can cause porosity. Degassing operations in aluminum melting reduce not only hydrogen but oxides as well. Filtration, which is commonly used in aluminum metal handling systems, has a well known effect of reducing porosity by reducing oxides. This increases the nucleation barrier for porosity formation.^(14, pp. 77-78) The nucleation of porosity by oxides has been demonstrated with late additions of machining chips or by stirring in the absence of inert gas. The oxygen content was higher in the "dirty" practice by an order of magnitude, over 100 µg/g compared to 10 µg/g, and the amount of porosity in the reduced pressure test doubled.^(15, p.85)

Copper alloys form porosity from hydrogen, moisture and carbon monoxide in nickel containing grades. Forming porosity often requires oxides to be present.

PINHOLES

Pinholes form when gas dissolved in the liquid metal becomes less soluble during solidification. This formation of small bubbles is due to reduced gas solubility and is similar to the bubbles formed in carbonated drinks when poured into a glass. The gas may be from dissolved gases in the melting and metal handling procedures or the result of exposure to a gas evolved from the mold, core or coating. Wet coatings or some chemical binder formulations result in a reaction with the solidifying metal causing porosity at the surface. Dirty or contaminated chills, poor sand binder mixing practices, failure to add iron

oxide in phenolic urethane binder systems, or condensation in the mold after closing are all well known causes of pinhole porosity.

Because the formation of pinholes is due to the lack of gas solubility, how soluble are gases in liquid metals? The partial pressure of gas for diatomic gases like hydrogen or nitrogen generally determines the solubility of gas in a liquid and can be calculated using Sievert's Law.

$$\text{Gas dissolved} = \text{Constant} * (\text{Partial Pressure of Gas in Atmosphere})^{1/2} \dots \text{Sievert's Law(G)}^{(3, p. 326)}$$

The solubility of gas in the liquid limits how much gas is dissolved during melting and handling. The dissolved amount of hydrogen in aluminum at equilibrium depends on the relative humidity, the partial pressure of hydrogen, and the temperature of the metal as shown in Figure 10.^(9, p. 3)

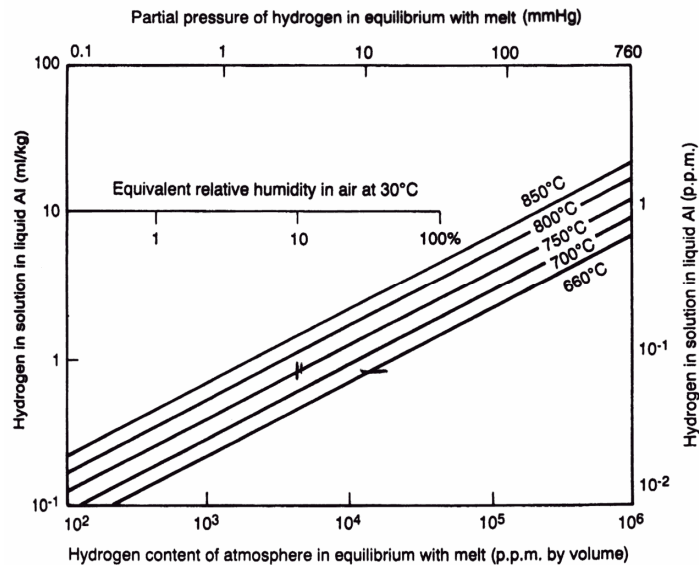


Figure 10. Hydrogen content of liquid aluminum at various temperatures.

Aluminum - The solubility of the gas decreases as the metal solidifies, as solidification reduces the space available for dissolved gas. The fall in solubility of hydrogen in aluminum at solidification is shown in Figure 11, falling from over 0.6 ml/100g or 6 ml/kg in the liquid to less than 0.1 ml/100g or 1 ml/kg in the solid.^(14, p. 74) The solubility of hydrogen at one atmosphere in pure aluminum in ml/ 100g is given as a function of temperature (°K) as:

$$\text{Ln (solubility ml/ 100g)} = -5872/T + 6.033 \text{ (H)}^{(14, p. 73)}$$

Applying Sievert's Law, equation G, the effect of the hydrogen partial pressure can be included:

$$\text{Dissolved Hydrogen (ml/ 100g)} = \text{Solubility (from H)} * P_{H_2}^{1/2} \text{ (partial pressure)} / f_H \text{ (activity)} \text{ (I)}^{(14, p. 73)}$$

The activity coefficient, in equation I, allows the effect of alloying elements on hydrogen solubility to be taken into account. Silicon, copper, manganese and nickel reduce the solubility of hydrogen. Pure aluminum has an activity coefficient of 1 but this increases for many common alloys; for example A356 has an activity coefficient of 1.48 and A319 has a coefficient of 1.78.

In comparison with the equilibrium-dissolved hydrogen in Figure 10, a relative humidity of 10% is enough to charge the aluminum with hydrogen. The internal equivalent gas pressure available for bubble formation can be estimated from Figure 10. For example, an aluminum casting poured at a temperature of 750°C (1382°F) at a relative humidity of 10% and a hydrogen partial pressure of 6 mm Hg or 0.008 atm contains about 0.9ml/kg hydrogen. The pressure while cooling increases

at this hydrogen concentration to 10.5 mm Hg or 0.013 atm. It only requires a little over 50 mm (2 in) of aluminum metalostatic head to suppress bubble formation without considering the added pressure needed for nucleation.

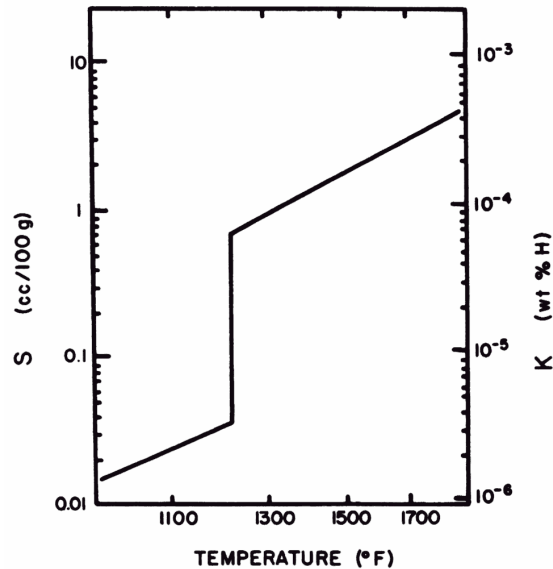


Figure 11. Solubility of hydrogen at one atmosphere in pure aluminum.

Aluminum melting operations typically result in hydrogen contents in excess of 0.20 ml /100 g. Good methods of degassing reduce the hydrogen to 0.06 to 0.10 ml /100 g.^(16, p. 890) Experience in aluminum casting production indicates that porosity does not occur with hydrogen levels below 0.15 ml/100g or 1.5 ml/kg. This is roughly the equivalent of 60 mm of Hg or 0.08 atm at solidification. The pressure to form a gas bubble must not only exceed the metalostatic head pressure, it must also overcome the nucleation barrier given in Equation D as $2\sigma/r$. Nucleation on oxide films reduce the needed pressure for porosity not only by increasing the initial radius, r , but also changing the surface tension requirement. In the case of heterogeneous nucleation, wetting angle and surface morphology is key. In aluminum castings, hydrogen porosity may not form up to 0.30 ml/100g if the aluminum is free from nucleating oxides. This increases the pressure to 0.13 atm at solidification to form porosity. As the aluminum melt is lower in oxides or hydrogen, porosity changes forming later in solidification. A study showing the change in porosity morphology is shown in Figure 12.^(18, p. 681)

The surface tension of liquid aluminum is about 900 dynes/cm. If the nucleation pressure is the primary pressure to be overcome, especially when the porosity forms late in solidification, then the nucleation size of the oxides can be calculated. At a pressure of 0.08atm, the equivalent pressure for hydrogen contents of 1.5 ml/kg, the nucleation size is 0.022 cm. For the clean aluminum nucleating pressure of 0.13 atm, the size is 0.013 cm (0.0005 in). These are not unreasonable sizes for nucleation sites for pinhole porosity in aluminum castings.

The composition of the gases evolved during pouring and solidification are given in Table 9.^(2, p. 683) The average composition at one minute may give some indication of the potential for contribution from the mold or core in forming pinhole porosity in aluminum castings. Hydrogen is only present at low levels suggesting that exposure to moisture in melting may be more important to hydrogen porosity in aluminum castings. Most of the gas appears to be escaping air as seen in the high levels of nitrogen and oxygen, from 60% to over 95%. The only significant other gas, carbon dioxide, is due to the combustion of the binder since carbon is not an alloy in aluminum. Hydrogen in the binder could be present in the moisture that was not recorded. In aluminum, binder decomposition may contribute to the dissolved hydrogen in the metal and not escape to be measured. The high levels of oxygen and carbon dioxide are evidence of the formation of an oxide film at the surface, protecting it from further oxidation and reducing the ongoing reduction of water with the subsequent pickup of hydrogen. If moisture is present, it can certainly cause local pinhole formation.

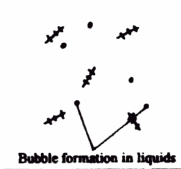
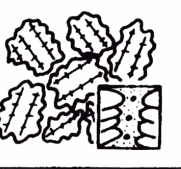
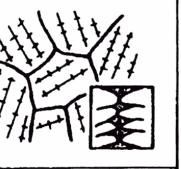
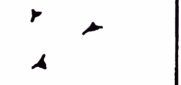
	1) round pores	2) long, broad pores	3) long, fissured pores	4) small, fissured pores
Solidification process and bubble formation	 Bubble formation in liquids			
Pore morphology in the structure				
Characterization	<ul style="list-style-type: none"> - precipitation in the liquid melt or in the beginning of solidification - unrestricted bubble growth - high H₂ concentration required 	<ul style="list-style-type: none"> - bubble formation with still high liquid fraction - arrangement between growing bubbles and dendrites - high to medium H₂ concentration 	<ul style="list-style-type: none"> - bubble formation during formation of the dendrite network - bubble expansion limited by still open melt channels - medium to low H₂ concentration 	<ul style="list-style-type: none"> - precipitation shortly before the end of solidification - shape and size of pores determined by closed interdendritic spaces - low H₂ concentration

Figure 12. Four types of pores in aluminum castings.

Table 9. Composition of Gas evolved in Aluminum Casting after One Minute

Binder /LOI	Hydrogen H ₂	Oxygen O ₂	Nitrogen N ₂	Carbon Monoxide CO	Carbon Dioxide CO ₂	Total Hydrocarbons
PUNB 1.78	ND	18.3	74.0	0.4	3.8	0.3
PUNB 1.78	ND	16.9	71.0	0.7	7.0	0.6
PUNB 3.07	ND	10.8	55.8	1.9	24.8	1.3
PUNB 3.07	1.3	10.6	51.3	2.4	27.1	2.0
FNB 1.89	ND	18.9	75.6	0.7	1.4	0.3
FNB 1.89	ND	20.0	77.3	0.3	0.4	0.1
FNB 2.57	0.4	13.7	65.9	4.9	9.7	2.3
FNB 2.57	ND	13.9	64.2	6.1	9.5	2.8

Copper – Careful melting practices, which include fluxing, degassing and deoxidation, are necessary if copper alloys are to be produced without gas porosity. As always, avoiding overheating and minimizing time at temperature in the melt minimizes gas pickup. Fluxing is used to prevent gas pickup during melting. This is especially true in combustion heating where both oxygen and hydrogen can be picked up depending on the alloy. Dissolved oxygen and hydrogen pick up are problems. Degassing may be necessary to avoid problems with these gasses. Copper alloys can have short, medium or long freezing ranges. It is common in some alloys to deoxidize to prevent porosity. Porosity can be due to the formation of steam from the reaction of dissolved hydrogen and oxygen. If oxygen is not available then porosity may be avoided. Oxygen may only be necessary for nucleation. Copper nickel alloys also form carbon monoxide since carbon is higher in these grades.^(19, p. 774-776)

To most copper alloy foundrymen, melt control is about getting rid of the gas. Like most metals, the solubility for gas in copper drops during solidification. In Figure 13, the solubility of hydrogen in copper and copper tin alloys is shown.^(20, p. 731) At solidification, the solubility falls from over 5 ml/ 100g to about 2 ml/ 100g. Dividing 100 g of copper by the density, 8.8 g/ml, gives 11.4 ml of copper. If the copper rejects 3 ml/ 100g, that would be 3 ml hydrogen in 11.4 ml of copper. This would correspond to 26% porosity. This volume is at STP and would be much higher at temperature. Using the more common weight percentage makes the level of hydrogen seem low; 3ml of hydrogen is 0.00067 g hydrogen in 100 g of copper, or 0.67 ppm. The hydrogen content of aluminum is expressed in a similar way for the same reason. During melting the hydrogen partial pressure is not 1 as in Figure 9 but some lower value. If we use a lower value such as 0.01 atm and apply Sievert's Law, equation G, this results in a calculated value of 0.5 ml/ 100g.^(20, p. 731)

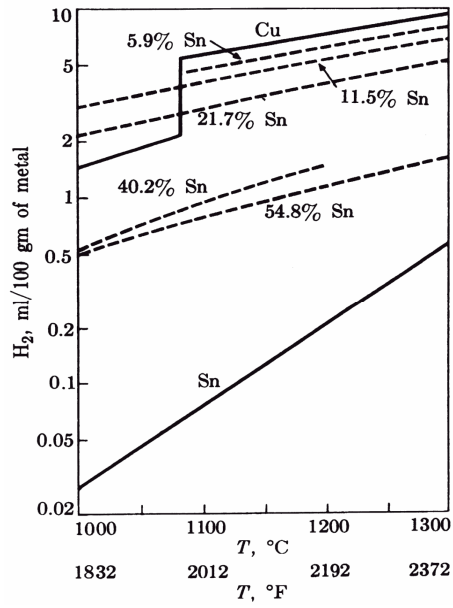


Figure 13. Solubility of hydrogen in copper, tin and copper-tin alloys.

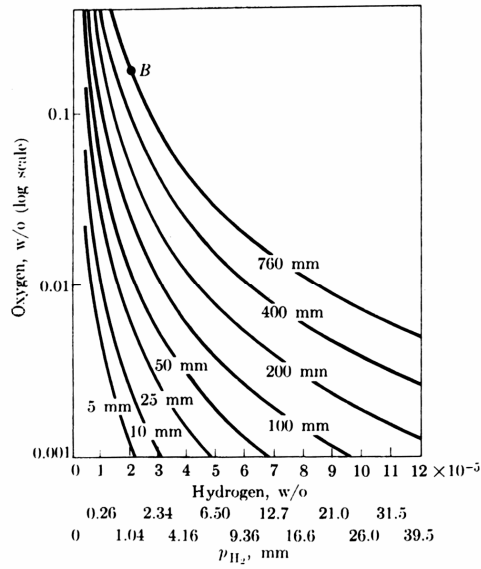


Figure 14. Equilibrium of water vapor with molten copper at 1083C.

As noted above, porosity is not simply the result of excess hydrogen but oxygen also plays a role. The equilibrium solubility of water vapor and molten copper is shown in Figure 14.^(20, p. 732) Higher oxygen contents reduce the hydrogen solubility. Melting in air, exposure to moisture, entrapment of dross can all lead to higher oxygen contents and an increased tendency to form hydrogen porosity. Gas can be removed mechanically, by purging with an inert gas or vacuum treating, or chemically, by adding phosphorus, titanium or other agents.^(21, p. 448)

Iron - Solubilities of hydrogen and nitrogen in iron are shown in Figure 15.^(22, p. 123) Like aluminum, the solubility of each gas is dependent on partial pressure of the gas and temperature of the metal. Similar to aluminum, the solubility decreases during solidification by almost a factor of 5. Nitrogen pinholes in cast iron form at as low as 80 ppm but thin sections may contain as much as 120 ppm before forming porosity.^(12, p. 642) Ductile iron contains less nitrogen and is not subject to nitrogen pinholes unless inappropriate binders or molding practices are used. Normal levels measured in cast iron for nitrogen include 0.005-0.014% for malleable, 0.004-0.007% for gray, 0.004-0.012 for ductile base and 0.003 to 0.008% for treated ductile. Nitrogen is well known to affect the solidification, mechanical properties, and machinability of cast iron.^(23, p. 433)

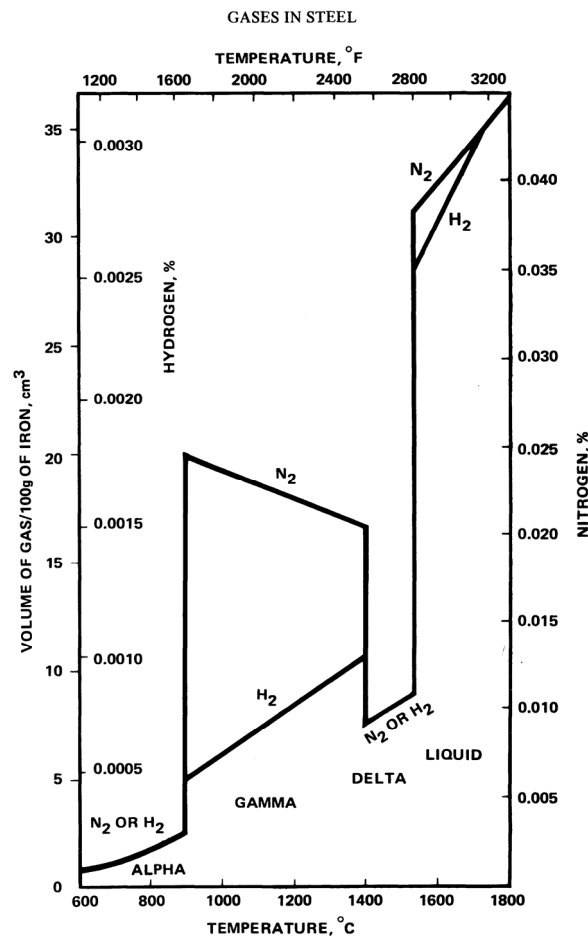


Figure 15. Solubility of hydrogen and nitrogen in iron at one atmosphere.

Solidification rate is obviously important in bubble formation for pinholes. Slow cooling rates allow the gas to escape before the liquid solidifies. Fast cooling rates may not allow enough segregation or time to form bubbles. Section sizes from 5 to 30 mm appear most prone to pinhole formation. Ductile iron appears more prone to pinhole formation than gray iron.

Hydrogen pinholes are often attributed to high aluminum content with as little as 0.005% in the melt associated with pinholes. Pinholes due to hydrogen are typically small ranging from 1 to 4 mm in diameter. The traditional explanation for pinholes in iron castings is the aluminum in the melt causes the moisture in green sand molds to disassociate and provide enough hydrogen to cause porosity. This is unlikely. Mold materials and melting practices can increase the hydrogen or decrease the nucleation pressure required affecting pinhole formation.

Prior work indicates that surface tension controls the formation of pinholes in iron castings. The surface tension was determined by measuring the pressure required to blow a bubble in iron. This surface tension was related to the metal composition and temperature, especially aluminum content. The surface tension is low in iron melts containing 0.015 to 0.15% aluminum. While aluminum greater than 0.2% will suppress pinholes, it degrades other mechanical properties. Other alloys like zirconium or rare earths can be added to increase surface tension and suppress porosity. The relationship, shown in Figures 16 and 17, is as expected from equation D, higher surface tension suppresses pinhole formation. ^(24, p. 374, 377)

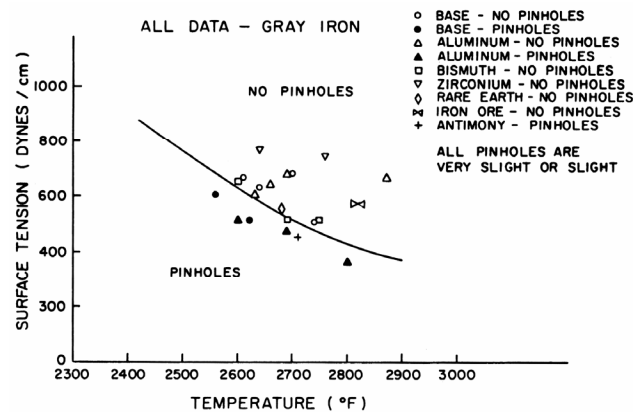


Figure 16. Surface tension vs. temperature in molten gray iron.

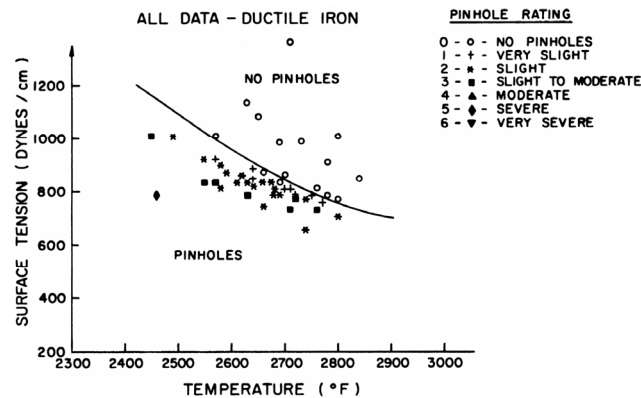


Figure 17. Surface tension vs. temperature in molten ductile iron.

The composition of gases evolved from chemically bonded sand mixtures are shown in Table 10. The levels of hydrogen are quite high. The nitrogen and oxygen are the air escaping and represent 20 to 30% of the gas evolved. The rough balance of carbon monoxide and carbon dioxide evidence the near equilibrium of carbon and oxygen at the mold metal interface.

Table 10. Composition of Gas Evolved in Iron Casting After One Minute

Binder /LOI	Hydrogen H ₂	Oxygen O ₂	Nitrogen N ₂	Carbon Monoxide CO	Carbon Dioxide CO ₂	Total Hydrocarbons
PUNB 1.78	36	5.7	22.7	11.4	15.3	8.8
PUNB 1.78	34	5.5	21.6	9.9	18.8	10.1
PUNB 3.07	35	4.8	19.8	20.3	13.9	5.1
PUNB 3.07	35	5.0	20.8	20.8	13.2	4.8
FNB 1.89	39	5.1	19.9	21.4	8.5	6.2
FNB 2.57	43	4.1	15.8	23.6	8.5	4.8
FNB 2.57	44	4.0	15.8	23.9	8.4	4.3

Different binder systems did not seem to be influential in earlier reported work but field experience has consistently shown that changes in binder type and even variations in binder formulation in production can lead to significant increases in pinhole formation. In more recent tests, several binder systems were evaluated for their tendency to form pinholes in gray iron. Phenolic hotbox with the greatest nitrogen content (8.5%) gave the most severe porosity. Two formulations of phenolic urethane with intermediate nitrogen (3.9%) gave less porosity while FRC Acrylic-Epoxy and ester cured Alkaline Phenolic had the least nitrogen (< 1%) and were free from pinhole porosity. The binder levels in the test were higher than production levels, 2% for the tests compared to 1% typical in practice. Both nitrogen and hydrogen were thought to contribute to pinhole formation.^(25, p. 493)

Pinhole porosity occurs in phenolic urethane bonded sand systems producing iron and steel castings unless iron oxide is added to the formulation. Iron oxide increases the possibility of blowholes. This is probably due to the small size of the iron oxide particles decreasing the permeability of the sand mixture. It will also increase the amount of gas to be removed due to any moisture included in the oxide and because of the release of oxygen by the oxide at high temperatures.^(7, p. 374) Some have attributed the reduction of pinhole porosity to the contamination of iron oxide with titanium oxide but this is thermodynamically implausible. Others have proposed that the iron oxide forms a glass film preventing the gas evolved during casting from reacting with the surface. A more likely explanation is the chemical action of the iron oxide in the sand mixture. As the temperature increases and the oxygen activity decreases, iron oxide releases some oxygen. It is not clear whether the reduction of iron oxide increases the oxygen on the liquid metal surface decreasing the absorption rate like the glass formation idea or if it combines with the gas to form nitrous oxide and prevent absorption.^(26, p. 355) Iron oxide, either red or black, is added to prevent porosity formation. It is also helpful in preventing porosity to balance the ratio of part I with part II, 50/50, or favoring part I over part II, 60/40. Favoring part II over part I increases porosity. Inadequate mixing time can lead to a higher incidence of porosity, likely due to non-uniform binder concentrations at the mold metal interface.^(27, p. 64)

Newer formulations of phenolic urethane have been tested to confirm the observations stated above. As seen in the earlier work, unbalanced ratios favoring part II continues to promote porosity. The unfavorable ratio may be due to a lack of mixing control or a desire to improve strength or facilitate stripping. Reducing the binder level in the sand mixture helped reduce porosity with trials showing significant reduced porosity when binder levels were changed from 3%, 1.8%, 1.5% and 1.25%. Reducing the pouring temperature from 1510°C (2750°F) to 1371°C (2500°F) reduced porosity. Most of the porosity in a step cone casting occurred between 2.2 cm (0.875 in) and 3.5 cm (1.375 in). Smaller section sizes may have shown surface pocking. Mixing times that were inadequate for uniform coating showed increased porosity with high levels at 10 s. and no porosity at 60 s. In iron, low carbon equivalents, 3.4% compared to 4.3% gave greater porosity. Additions of slight amounts of zirconium or titanium eliminated porosity. Iron oxide additions eliminated porosity even at 0.25% when red iron oxide was used.^(28, p. 850)

Steel - To avoid pinholes in steel, hydrogen contents in casting should remain under 6 ppm or 0.0006%. Porosity occurs in the range of 9 to 13 ppm with porosity always present at levels in excess of 13 ppm. Hydrogen is picked up in melting. Hydrogen problems in steel casting production are most problematic in alloys containing nickel especially low temperature or high strength grades. Hydrogen is responsible for loss of ductility in tensile tests and can be reduced by low temperature baking. Hydrogen is thought to be responsible for wormhole like porosity that originates at the surface and extends toward the thermal center of the casting. The occurrence of hydrogen related problems also seems to be dependent on relative humidity and therefore more common in more temperate regions. This can be seen in some seasonal trends in Figures 18 and 19.^(22, p. 270-271)

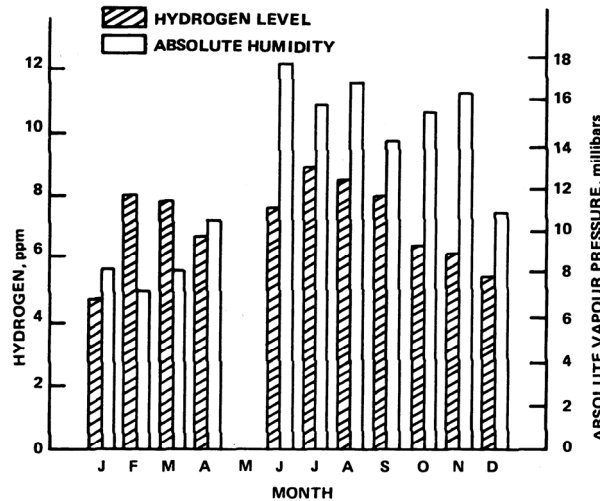


Figure 18. Variation of humidity and hydrogen in steel for a period of one year.

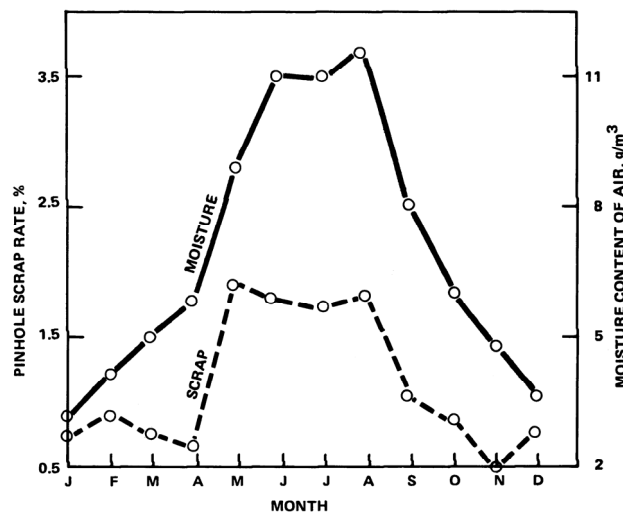


Figure 19. Variation in moisture content and pinhole scrap in steel for a period of one year.

With lower carbon levels than iron and added deoxidizers coupled with the higher temperature of casting for steel, the gases evolved have the highest carbon monoxide and hydrogen levels. The higher gas evolution rate is also seen in the lower oxygen and nitrogen combined levels from 13 to 20%. The composition of gases evolved in steel casting with various sand formulations is given in Table 11.

The composition of gases evolved can be compared to the equilibrium ratios given in Figure 20.^(3, p.358) For example from Table 11, the ratio of carbon monoxide to carbon dioxide varies from 2 to 10. This is close to the equilibrium value but on the oxidizing side for iron-iron oxide at the steel melting point. Cast iron had ratios from .5 to 2 in Table 10, again close to equilibrium but on the reducing side. This may be due to the higher carbon content or lower temperatures. As long as the iron-based alloy is molten the interface will trend toward equilibrium and react with gases to achieve that condition. Aluminum in Table 9 shows little correlation to Figure 20, due in part to the oxide film that forms at the interface so that the composition of the gases evolved are not as influenced by the molten metal.

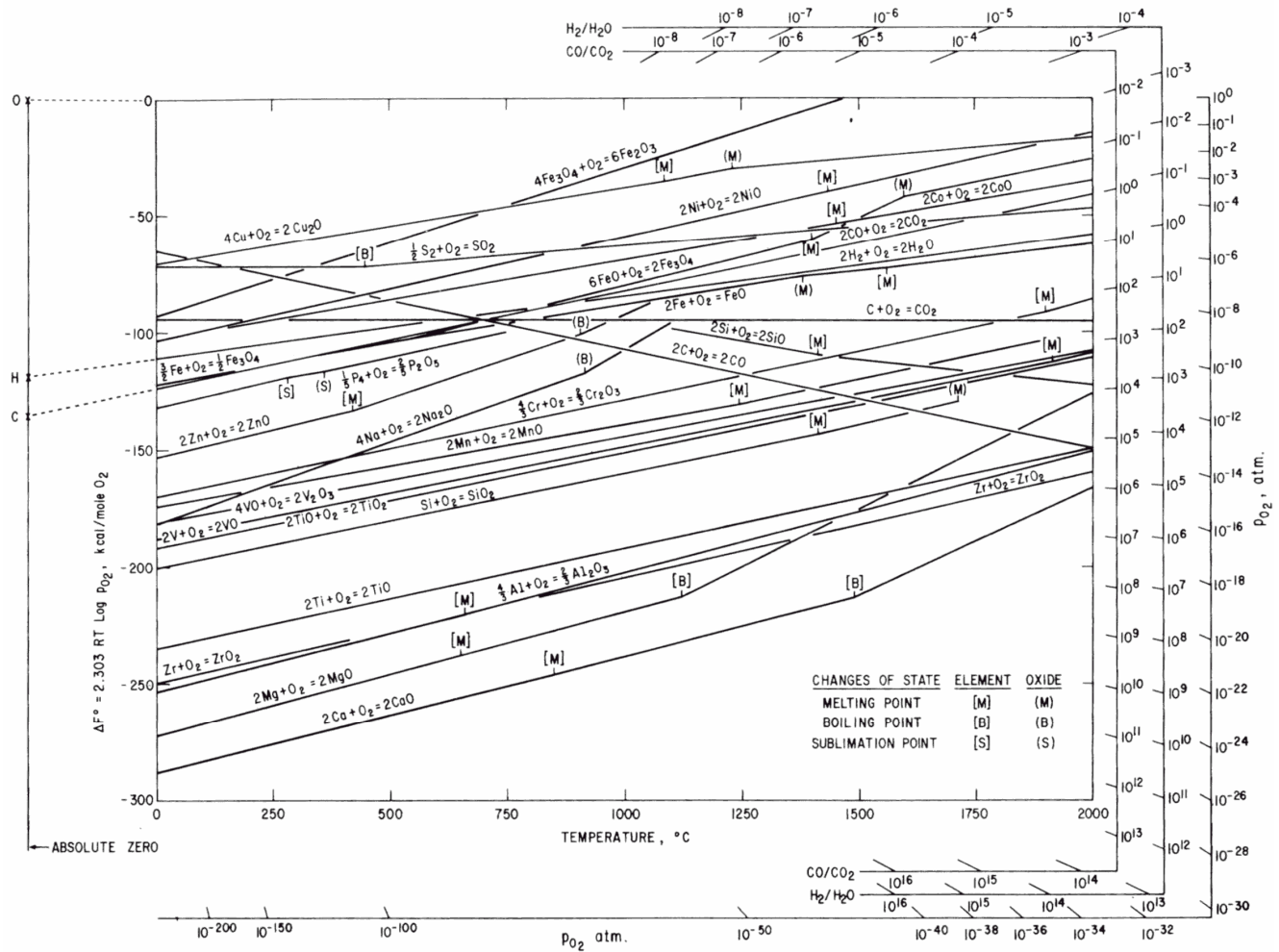


Figure 20. Free energy of formation of oxides for standard states.

Table 11. Composition of Gas Evolved in Steel Casting After One Minute

Binder /LOI	Hydrogen H ₂	Oxygen O ₂	Nitrogen N ₂	Carbon Monoxide CO	Carbon Dioxide CO ₂	Total Hydrocarbons
PUNB 1.78	45	4.0	16.0	21.8	10.1	2.8
PUNB 1.78	44	3.8	16.9	25.4	7.9	2.0
PUNB 3.07	40	2.4	10.8	34.3	10.1	2.4
PUNB 3.07	46	2.8	13.5	27.6	8.6	1.8
FNB 1.89	46	2.9	11.9	31.8	4.4	2.7
FNB 1.89	46	3.2	12.7	32.2	3.3	2.1
FNB 2.57	45	3.0	11.4	32.9	4.9	2.8
FNB 2.57	45	3.0	12.4	33.7	3.7	2.5

Pinholes can also form from nitrogen in steel casting so the nitrogen contents should remain under 120 ppm or 0.0012%. Nitrogen is more of a problem in chromium containing grades of steel. The heating of chromium additions in a cold charge allows significant pickup of nitrogen from the air. Chromium increases both the rate of nitrogen pickup and the solubility of nitrogen. The oxygen blow in arc melting practices reduces the hydrogen and nitrogen contents of the steel. Nitrogen levels are elevated by reheating in arc melting after deoxidation. The use of nitride formers such as zirconium or titanium is often used to avoid problems with nitrogen. They should be added after primary deoxidation to prevent the oxidation of these nitride formers. Adding as little as 0.1% zirconium after aluminum deoxidation to CA6NM has been shown to prevent porosity formation.^(29, p. 118)

The nitrogen content in steel during melting in an acid-lined electric arc furnace has been studied. Typical melt cycle nitrogen content is shown in Figure 21. Control of nitrogen requires minimizing the nitrogen in the melt charge, maintaining at least 0.30% silicon in the charge, a carbon boil of at least 0.30%, using lower voltage settings later in the heat, and minimizing exposure through compact streams and rapid tapping.^(30, p. 23)

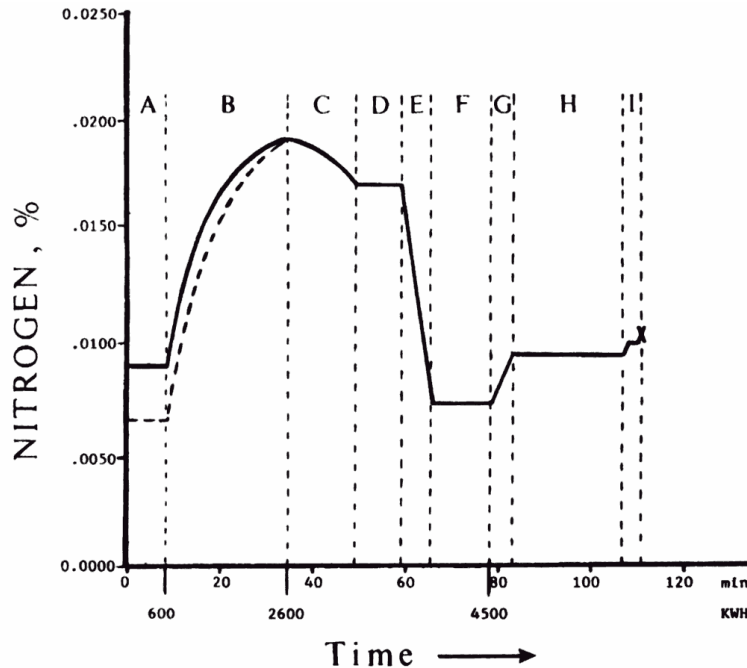


Figure 21. Nitrogen content during the entire steelmaking process. Lettered areas correspond to the following legend: A = electrodes boring through a cold charge; B = small molten pool forms and grows with #1 tap; C = remaining charge melted with #2 tap; D = bath heated to carbon boil temperature; E = carbon boil period; F = ferroalloy additions made and bath heated to tapping temperature on #2 tap; G = tapping of the heat; H = molten steel held in tap ladle; I = molten steel reladled and cast.

The surface tension, σ , of liquid steel is about 1500 dynes/cm. The radius of iron atoms is 1.26 Angstroms or 1.26×10^{-8} cm. To form a gas bubble equivalent to ten atomic radius of iron would require $2\sigma/r$ or 2.4×10^{11} dynes/cm² or 235,000 atm. If an inclusion provides a nucleation site that is 10^{-2} cm then the required pressure drops to 0.15 atm. Nucleation is required for formation of bubbles. Blowholes have large mold features to initiate from so nucleation pressures are insignificant. Pinholes may be quite small and if they form inside the casting, the nucleation pressure can be significant.

Pinholes are more prevalent in thinner castings with 10 to 30 mm (0.4 to 1.2 in) wall thickness. In the blowhole experiments, bubbling in aluminum or iron resulted in large single bubbles but in steel a more general pinhole like porosity formed. Pouring temperature appears to have little effect. Higher moisture contents in molding sands and higher relative humidity gives more pinholes.^(19, p. 254) Pinholes are typically small, 1 to 2 mm (0.04 to 0.08 in) in diameter. Moisture on chills, inadequately dried coatings, improperly mixed sand can all cause pinhole formation.

Different alloys have different susceptibility to pinhole formation depending on the solubility of gas in the liquid and solid. Experience in remelting AOD ingots in induction furnaces shows the tendency to form pinholes for several alloys as shown in Table 12.^(31, p. 1018)

Table 12. Tendency for Steel Alloys to Form Pinholes

High	Medium	Low
Carbon Steel	Tool Steel	Mn Steels
Low Alloy Steel	CA Type (400 series)	CF Type (300 series)
Silicon Irons	CB Type (PH series)	Duplex Stainless
50-50 Alloys	Cast Iron	Nickel base
CZ 100 (cast nickel)		Cobalt Base
Ni-Cu Alloys (Monel)		N-155

SHRINKAGE

Solidification shrinkage occurs as the liquid metal becomes a more dense solid. To form, shrinkage must form porosity and is subject to the same requirements as other porosity to form. While we think of centerline shrinkage as a thermal solidification pattern event, the actual formation is a porosity pressure driven event. If the solidification is progressive because of favorable casting design, the riser level drops as the liquid metal is pulled into the solidifying casting. This is just like a blowhole formation without a metallostatic head to overcome and normal atmospheric pressure providing the gas.

When feeding is cut off and the metal continues to solidify the pressure in the remaining metal pool decreases while segregation causes the gas content to increase. In thin walls the shrinkage may result in cavitation of the walls. Where there are hot spots touching the mold, shrinkage will start at the mold and form like a blowhole but the pressure in the liquid will drop below atmospheric as the metal solidifies. In centerline shrinkage, the porosity must be nucleated and gas must be available.

Porosity in aluminum alloys is the result of hydrogen and is controlled by the dissolved hydrogen, presence of nucleation sites or oxides, and the conditions of solidification. (32, p. 961) Modification of aluminum-silicon alloys with strontium can change the solidification pattern and result in more microporosity and less macroporosity. Some operations have used this to try and reduce the harmful effects of hydrogen in these alloys. (33, p. 71) The gas pore size is a result of the cooling rate, gas content and solidification pattern as shown in Figure 22 (34, p. 995)

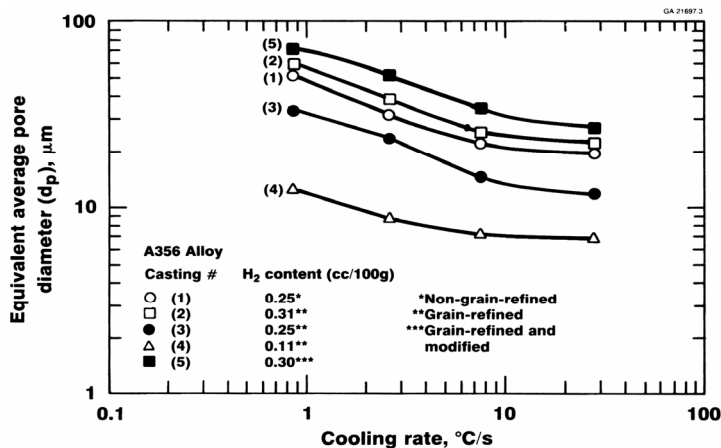


Figure 22. Average pore diameter as a function of cooling rate in cast aluminum A356.

The combination of low pressures, segregation of gas and other elements leads to a combination of solidification and gas porosity in copper alloys. (19, p. 733)

Avoiding shrinkage porosity has been controlled using an engineering approach based on modulus and volume. Modulus is the volume divided by surface area or crudely the heat to be removed by the rate of removal. The ratio of the riser volume to casting volume and the ratio of riser modulus to casting modulus are used to determine if the configuration will exhibit shrinkage. Surprisingly, this approach has been shown to work on alloy systems as diverse as ductile iron, aluminum-silicon, and steel. For a volume ratio of one, iron and steel require a modulus ratio of about 1.2 while the aluminum alloy required a ratio of 1.7 as shown in Figure 23. (35, p. 470)

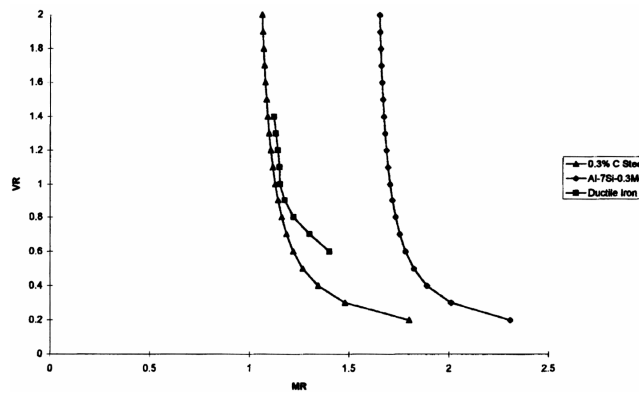


Figure 23. VR vs. MR relation for three cast alloys.

Predicting shrinkage has relied on predicting isolated hot spots. The use of solidification models with numerical thermal criteria like Niyama has been successful at dramatically improving casting quality and soundness of design. The solidification models have not predicted porosity because it depends on nucleation and gas availability. Recent developments in solidification modeling coupling liquid flows and pressure fields have shown promise in the shrinkage porosity prediction. These models include Sievert's Law, nucleation, pressures, feeding flows in the liquid, and the gas concentrations. The inclusion of porosity models should predict pinholes as well as the solidification shrinkage.^(36,37)

Pressurized risers could dramatically extend feeding distances by suppressing porosity formation and providing liquid to more remote areas of the casting. In skin forming alloys like steel, the riser can be pressurized after the riser neck is sufficiently solid and more effectively feed the casting and prevent centerline shrinkage. Initial trials of pressurized risers have shown promise and work is continuing.⁽³⁶⁾

POROSITY AND PERFORMANCE

Designers are uncertain how to account for porosity in their casting designs. They can specify extensive quality tests, perform extensive performance testing, and use large factors of safety. All of these methods do not necessarily guarantee performance and they are all somewhat costly. Different industries use combinations of these strategies to try to create robust cost effective designs.

The detection of porosity through nondestructive inspection is common. Unfortunately, often the porosity in the critical sections might be so minor that it is not detected and yet still limit critical performance. Even if detectable, the quality standards available for characterizing porosity are qualitative. Most are subjective workmanship standards that are unable to ensure performance. A recent study on radiography showed that when 128 films were rated in 5 X-ray levels, the one sided 95% confidence interval was 1.42 levels. Systemic porosity like shrinkage can be managed better than chaotic porosity like pinholes.⁽³⁸⁾

Performance testing can be used to establish limits on high production items and used to relate porosity and performance. This allows the designer to specify the allowable limits and inspections. This is costly and may fail to avoid failures if the testing fails to replicate the service performance requirements.

Large factors of safety limit the effectiveness of design. The thicker section sizes, increase in mass, and change in geometry may create porosity that was not present in smaller components. This trade off of size and safety is less clear than is often assumed.

Porosity and microshrinkage in aluminum castings limit the mechanical properties of the alloys. Porosity as a function of hydrogen content is shown in Figure 24 and the resulting reduction in strength is shown in Figure 25.^(19, p. 747) Cast aluminum has limited ductility so small amounts of porosity can have a large effect on strength.

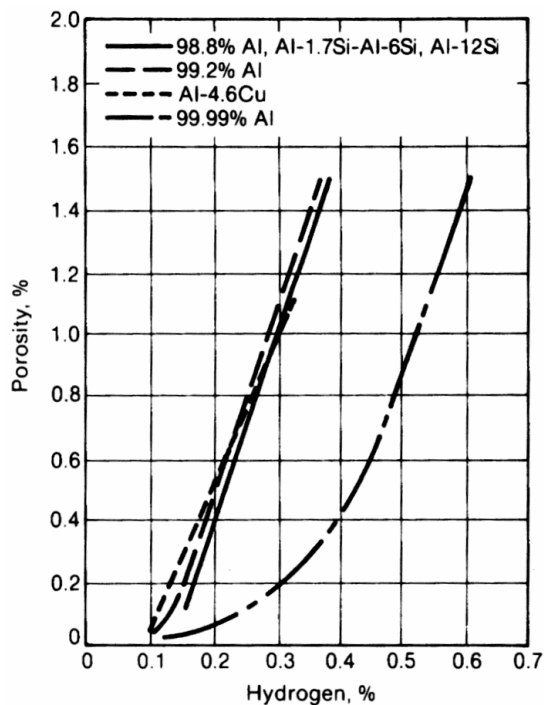


Figure 24. Porosity as a function of hydrogen content in cast aluminum.

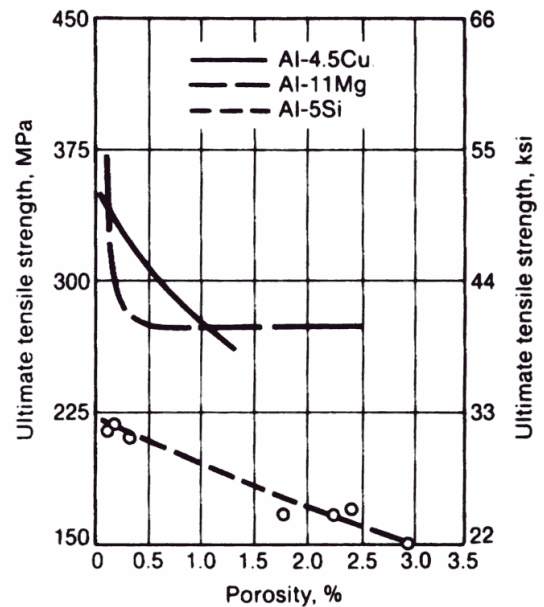


Figure 25. Ultimate tensile strength vs. hydrogen porosity for cast aluminum.

Microporosity in steel castings as a result of shrinkage has been shown to be predicted in solidification modeling through the application of the Nyama criteria. Lower values of Nyama increase the likelihood of porosity. Nyama Criterion has been shown to correlate with X-ray level as shown in Figure 26 with values less than 0.2 producing castings with shrinkage detectable by radiography.⁽³⁸⁾ Values of Nyama up to 2 some reduction of strength but values above 2 have no effect on strength as seen in Figure 27.⁽³⁸⁾ Elongation seen in Figure 28 is dramatically effected by porosity.⁽³⁸⁾

One approach to determining performance based on porosity is to evaluate the component performance using finite element analysis (FEA) and reduce the modulus based on the percent porosity. Figure 29 shows some preliminary results in fatigue using this approach.⁽³⁸⁾

ACKNOWLEDGMENTS

I started in metal casting at Southern Research Institute with a wonderful group of friends that helped me immensely. They were fun and we were doing interesting and challenging work. Charles Bates had formed the team and provided leadership and direction. Bill Scott constantly challenged the conventional wisdom and was always pushing with innovative experiments. Jim Wren pushed to continue to experiment to verify all of our conclusions and speculations. Ruby James and Pat Goodman were essential in conducting the experiments, doing the chemical-analytical work and providing the chemistry needed to understand what was going on at the mold metal interface. Colt Pears demanded that the work stand up to critical scrutiny and provide sound technical data.

I am also blessed with great friends in the industry that helped me with this paper and this work. Ezra Kotzin always helped from the very beginning of my involvement in the industry. Rod Naro extended the original work and helped with this paper through our discussions and arguments. Christoph Beckermann, Von Richards, John Griffin and Charles Monroe reviewed the paper and made fundamental contributions that dramatically increased its value and accuracy. Finally, Malcolm Blair is a trusted coworker and sharp critic that helped formulate these ideas and constantly provides insights and improvements.

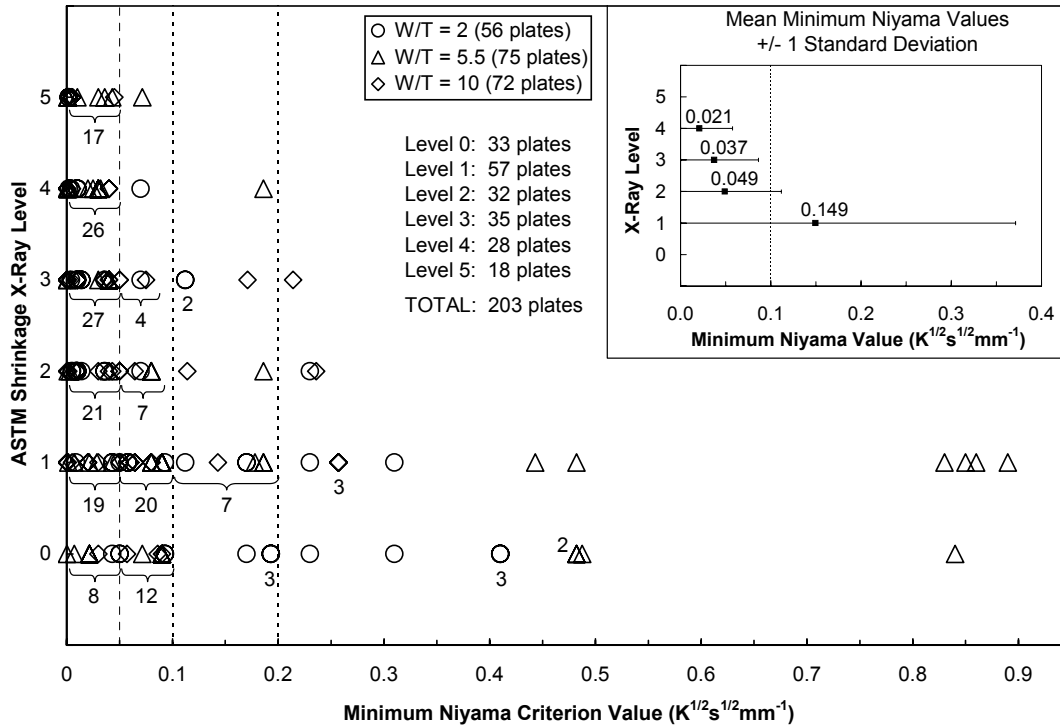


Figure 26. ASTM shrinkage x-ray level vs. minimum Niyama criterion value for the $W/T = 2, 5.5$ and 10 plates.

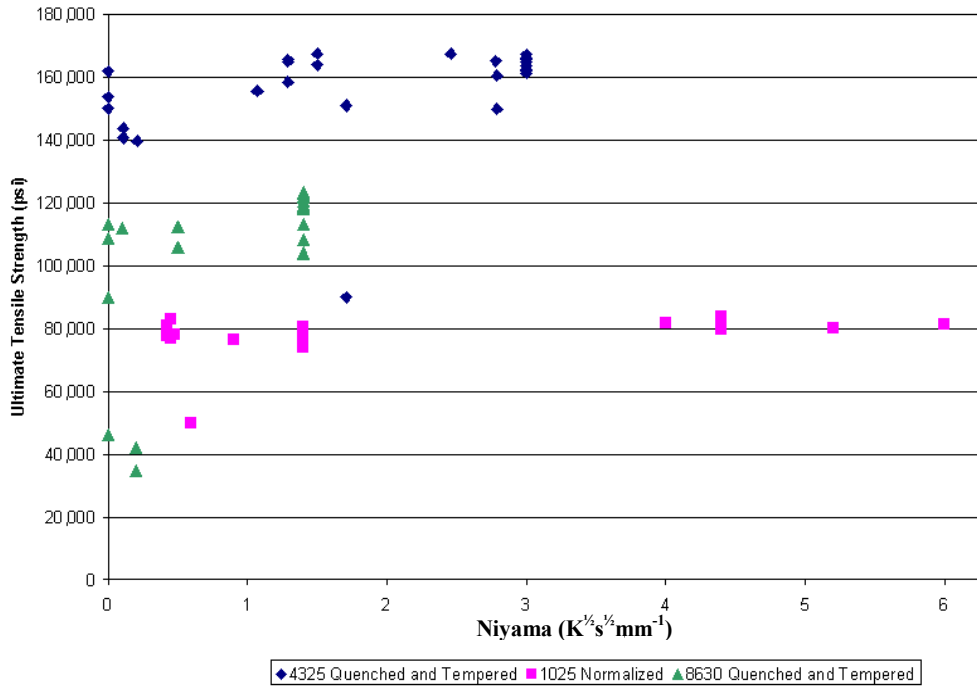


Figure 27. Effect of Niyama value on ultimate tensile strength.

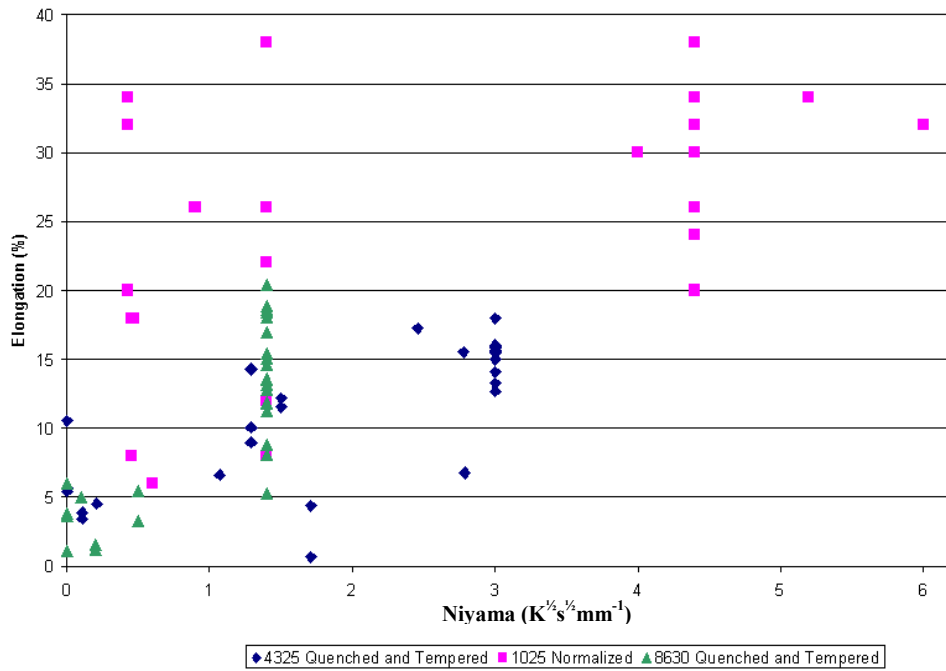


Figure 28. Effect of Niyama value on elongation.

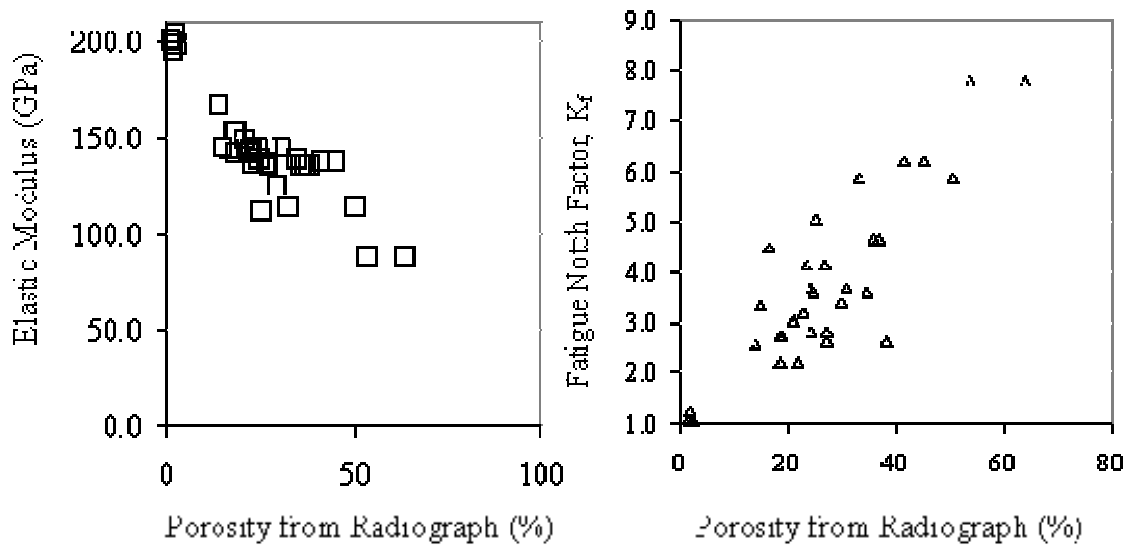


Figure 29. Measured relations between porosity in cast steel test specimens and (left) the elastic modulus and (right) the fatigue notch factor determined from test lives of specimens; the porosity percentage is indicative of the size of the cavity in the test specimens.

REFERENCES

1. C.E. Bates, R. W. Monroe, and J. Wren, "Mold Binder Decomposition and its Relation to Gas Defects In Castings," presented at the 1980 AFS Casting Congress, April 25, 1980.
2. C.E. Bates and R.W. Monroe, "Mold Binder Decomposition and its Relation to Gas Defects in Castings," *AFS Transactions*, vol. 89, pp.671-686, 1981.
3. *The Making, Shaping, and Treating of Steel*, USS, Ninth Ed., pp 281-402, 1971.
4. *Metalcaster's Reference and Guide*, American Foundry Society, 1972.
5. W.D. Scott, P.A. Goodman, and R.W. Monroe, "Gas Generation at the Mold-Metal Interface," *AFS Transactions*, vol. 86, pp.599-610, 1978.
6. *AFS Mold and Core Test Handbook*, American Foundry Society, 1978.
7. R.L. Naro and R.L. Pelfrey, "Gas Evolution of Synthetic Core binders: Relationship to Casting Blowhole Defects," *AFS Transactions*, vol. 91, pp. 365-376, 1983.
8. R. Monroe, "Mold metal Interactions: Gas Holes in Steel Castings," *Steel Founders' Research Journal*, Issue 3, pp. 5-12, 1983.
9. John Campbell, *Castings*, Butterworth-Heinemann, 1997.
10. W. Sun and C. Bates, "Visualizing Defect Formation in Gray Iron Castings Using Real Time X-rays," *AFS Transactions*, vol. 111, pp.1-8, 03-092, 2003.
11. R. Johns, "Designing Castings to Avoid Foundry Defects," *AFS Transactions*, vol. 88, pp. 199-208, 1980.
12. *Marks' Mechanical Engineers' Handbook*, Sixth Edition, McGraw-Hill, 1958, p.4-66 .
13. E.F. Ryntz, R.E. Schroeder, W.W. Chaput, and W.O. Rassenfoss, "The Formation of Blowholes in Nodular Iron Castings," *AFS Transactions*, vol. 91, pp. 161-164, 1983.
14. G.K. Sigworth, "A Scientific Basis for Degassing Aluminum," *AFS Transactions*, vol. 95, pp. 73-78, 1987.
15. G. Laslaz and P. Laty, "Gas Porosity and Metal Cleanliness in Aluminum Casting Alloys," *AFS Transactions*, vol. 99, pp. 83-90, 1991.
16. E.R. Kaczmarek, R. Leitermann, and R.W. Heine, "Pinhole and Slag Casting Defects in Ductile Iron Processing," *AFS Transactions*, vol. 105, pp.67-75, 1997.
17. S.A. Levy, "Evaluation of Molten Metal Quality for Aluminum Alloys," *AFS Transactions*, vol. 93, pp. 889-894, 1985.
18. X.-G. Chen and S. Engler, "Formation of Gas Porosity in Aluminum Alloys," *AFS Transactions*, vol. 102, pp. 673-682, 1994 .
19. *ASM Metals Handbook: Ninth Edition, Volume 15, Casting*, ASM, 1988.
20. P.K. Trojan, R.A. Flinn, and T.R. Ostrom, "Melt Control Variables in Copper-Base Alloys," *AFS Transactions*, vol. 90, pp. 729-744, 1982.
21. D.V. Neff, "Fluxing, Degassing, and Deoxidation of Copper-Base Alloys," *AFS Transactions*, vol. 97, pp. 439-450, 1989.
22. W.J. Jackson and M.W. Hubbard, *Steelmaking for Steelfounders*, SCRATA, 1979.
23. J.D. Farquhar, "Nitrogen in Ductile Iron-A Literature Review," *AFS Transactions*, vol. 87, pp.433-438, 1979.
24. R.V. Naik and J.F. Wallace, "Surface Tension – Nucleation Relations in Cast Iron Pinhole Formation," *AFS Transactions*, vol. 88, pp. 367-388, 1980.
25. D.M. Gilson, "The Role of Different Core Binder Systems in Iron Casting Production: Effect of Porosity Defects and Casting Properties," *AFS Transactions*, vol. 101, pp. 491-496, 1993.
26. R.W. Monroe, "Use of Iron Oxide in Mold and Core Mixes for Ferrous Castings," *AFS Transactions*, vol. 93, pp. 355-364, 1985.
27. R.L. Naro and J.F. Hart, "Phenolic Urethane no-Bake Binders: Ten Years of Progress," *AFS Transactions*, vol. 88, pp. 57-99, 1980.
28. R.L. Naro, "Porosity Defects in Iron Castings From Mold Metal Interface Reactions," *AFS Transactions*, vol. 107, pp. 839-851, 1999.
29. S. Kuyucak, "Prevention of Nitrogen Porosity in High-Chrome Steel Castings," *AFS Transactions*, vol. 102, pp. 117-120, 1994.
30. C.F. Pilliod, "Variables Affecting the Nitrogen Content of Carbon and Low-Alloy Acid Electric Arc Furnace Steels," *AFS Transactions*, vol. 100, pp. 23-25, 1992.
31. T. Klemp III, "A Simplified Approach to Degassing of Common Investment Casting Alloys," *AFS Transactions*, vol. 97, pp. 1009-1024, 1989.
32. E.L. Rooy, "Hydrogen: The One-Third Solution," *AFS Transactions*, vol. 101, pp. 961-964, 1993.
33. D. Argo and J.E. Gruzleski, "Porosity in Modified Aluminum Alloy Castings," *AFS Transactions*, vol. 96, pp.65-73, 1988.
34. Q.T. Fang and D.A. Granger, "Porosity Formation in Modified and Unmodified A356 Alloy Castings," *AFS Transactions*, vol. 97, pp. 989-1000, 1989.

35. J.T. Berry, R.P. Taylor, and R.A. Overfelt, "Porosity Patterns in A356 Bar and Plate Castings and Their Relation to Riser Design," *AFS Transactions*, vol. 105, pp.465-471, 1997.
36. K.D. Carlson, Z. Lin, R.A. Hardin, and C. Beckermann, "Modeling of Porosity Formation and Feeding Flow in Steel Casting," SFSA 56th Technical and Operating Conference, November 2002.
37. K.D. Carlson, Z. Lin, R. Hardin, C. Beckermann, G. Mazurkevich, and M. Schneider, "Modeling of Porosity Formation and Feeding Flow in Steel Casting," *Modeling of Casting, Welding, and Advanced Solidification Processes X*, ed. D. Stefanescu et.al., TMS, Warrendale, PA, 2003, pp. 295-302.
38. M. Blair, R. Monroe, C. Beckermann, R. Hardin, K. Carlson, C. Monroe, and J. Griffin, "Designing Reliable Castings," *Shape Casting: The John Campbell Symposium*, TMS, 2005.